REPORT DOCUMENTATION PAGE

Form Approved
OMB No. 0704-0188

1. REPORT DATE *(DD-MM-YYYY)*	**2. REPORT TYPE**	**3. DATES COVERED** *(From - To)*
June 2014	Technical Paper	June 2014- July 2014

4. TITLE AND SUBTITLE

Combustion Dynamics Behavior in a Single-Element Lean Direct Injection (LDI) Gas Turbine Combustor

5a. CONTRACT NUMBER
In-House

5b. GRANT NUMBER

5c. PROGRAM ELEMENT NUMBER

6. AUTHOR(S)

Huang, C., Gejji, R., Anderson, W., Yoon, C. and Sankaran, V.

5d. PROJECT NUMBER

5e. TASK NUMBER

5f. WORK UNIT NUMBER
Q12J

7. PERFORMING ORGANIZATION NAME(S) AND ADDRESS(ES)

Air Force Research Laboratory (AFMC)
AFRL/RQR
5 Pollux Drive
Edwards AFB CA 93524-7013

8. PERFORMING ORGANIZATION REPORT NO.

9. SPONSORING / MONITORING AGENCY NAME(S) AND ADDRESS(ES)
Air Force Research Laboratory (AFMC)
AFRL/RQR
5 Pollux Drive
Edwards AFB CA 93524-7013

10. SPONSOR/MONITOR'S ACRONYM(S)

11. SPONSOR/MONITOR'S REPORT NUMBER(S)
AFRL-RQ-ED-TP-2014-209

12. DISTRIBUTION / AVAILABILITY STATEMENT
Distribution A: Approved for Public Release; Distribution Unlimited

13. SUPPLEMENTARY NOTES
Technical paper presented at 50th AIAA/ASME/SAE/ASEE Joint Propulsion Conference, Cleveland, OH, 28-30 July, 2014.
PA#14363

14. ABSTRACT

A concurrent computational and experimental study of self-excited combustion dynamics in a model configuration of a lean direct injection (LDI) gas turbine combustor is described. Incoming air temperature and equivalence ratio were varied. Simulation at low equivalence ratio compared better with measurement and thus this condition was selected for a more detailed study of the underlying combustion dynamics mechanisms. First, hydrodynamic modes are investigated by conducting the simulation with an acoustically-open combustor so that acoustic effects on the flow field are minimized. The Vortex Breakdown Bubble (VBB) proves to be an important flow structure that can easily interact with the acoustic field to sustain instability. Second, detailed cycle studies of the acoustically closed combustor simulation reveals enhanced mixing and vaporization of the JP-8 fuel spray due to acoustic compression wave. Dynamic Mode Decomposition (DMD) analysis is used to identify the coupling between axial acoustics and the vortex breakdown bubble in the lower frequency region. Presence of another important hydrodynamic mode, the Precessing Vortex Core (PVC) is also identified from the DMD analysis. The possibility of nonlinear coupling between the acoustics and PVC modes is indicated.

15. SUBJECT TERMS

16. SECURITY CLASSIFICATION OF:			**17. LIMITATION OF ABSTRACT**	**18. NUMBER OF PAGES**	**19a. NAME OF RESPONSIBLE PERSON**
					V. Sankaran
a. REPORT	**b. ABSTRACT**	**c. THIS PAGE**	SAR	26	**19b. TELEPHONE NO** *(include area code)*
Unclassified	**Unclassified**	**Unclassified**			661-275-5534

Standard Form 298 (Rev. 8-98)
Prescribed by ANSI Std. 239.18

Combustion Dynamics Behavior in a Single-Element Lean Direct Injection (LDI) Gas Turbine Combustor

Cheng Huang[1], Rohan Gejji[2], William Anderson[3]
Purdue University, West Lafayette, IN, 47907

Changjin Yoon[4]
GE Global Research Center, Niskayuna, NY 12309

and

Venkateswaran Sankaran[5]
Air Force Research Laboratory (AFRL), Edwards AFB, CA, 93524

A concurrent computational and experimental study of self-excited combustion dynamics in a model configuration of a lean direct injection (LDI) gas turbine combustor is described. Incoming air temperature and equivalence ratio were varied. Simulation at low equivalence ratio compared better with measurement and thus this condition was selected for a more detailed study of the underlying combustion dynamics mechanisms. First, hydrodynamic modes are investigated by conducting the simulation with an acoustically-open combustor so that acoustic effects on the flow field are minimized. The Vortex Breakdown Bubble (VBB) proves to be an important flow structure that can easily interact with the acoustic field to sustain instability. Second, detailed cycle studies of the acoustically closed combustor simulation reveals enhanced mixing and vaporization of the JP-8 fuel spray due to acoustic compression wave. Dynamic Mode Decomposition (DMD) analysis is used to identify the coupling between axial acoustics and the vortex breakdown bubble in the lower frequency region. Presence of another important hydrodynamic mode, the Precessing Vortex Core (PVC) is also identified from the DMD analysis. The possibility of nonlinear coupling between the acoustics and PVC modes is indicated.

I. Introduction and Objectives

Prediction of combustion dynamics through high-fidelity simulations is necessary to develop a new generation of low emission gas turbine combustors as their narrow, lean operational regime makes them susceptible to combustion instabilities. Lean Direct Injection (LDI) is one concept for lean-burning, low NOx, liquid-fueled gas turbine combustors. In the LDI combustor, fuel is injected into a highly inertial and swirling air flow accelerated by a converging-diverging subsonic venturi to achieve a high degree of premixedness.[1-3] Simulations tested by experiment can provide the detail that is needed to understand the complex physics comprising the interacting modes of hydrodynamics, acoustics, and combustion in the multi-phase flow. As part of the present work, concurrent experimental and computational studies are conducted on a single element LDI combustor to assess the capability of high fidelity simulations to predict measured low-level, self-excited combustion dynamics.

---

1 Graduate Research Assistant, School of Mechanical Engineering and Student Member AIAA.

2 Graduate Research Assistant, School of Mechanical Engineering and Student Member AIAA.

3 Professor, School of Aeronautics and Astronautics and Associate Fellow AIAA.

4 Combustion Dynamics Research Engineer, Combustion Dynamics and Diagnostics Lab, GE Global Research Center and Member AIAA

5 Senior Scientist, Rocket Propulsion Division and Senior Member AIAA.

The flow-field and NOx emissions in the LDI combustor have been studied by a number of groups over the past several years.[4-9] A few studies at lower chamber pressure (~0.3 MPa) have investigated combustion dynamics. Santavicca et al[10-12] studied a Jet-A fueled combustor with pressure fluctuations amplitudes as high as 8% of the mean chamber pressure and measured the temporal and spatial CH*-chemiluminescence downstream of the combustor dump-plane. A large dependence of equivalence ratio, incoming air flow rate and air temperature was reported on the flame transfer function (FTF). It is interesting to note that the observations were similar to those made in lean premixed, low-pressure gas systems.[13,14]

Swirl stabilized combustion is presently common in gas turbine combustors. Combustion dynamics in swirl stabilized flames have been attributed to swirl-acoustic interactions.[15,16] Candel et al[17-19] reported a non-linear interaction between the hydrodynamic precessing vortex core (PVC) mode and the thermo-acoustic modes in the combustor in premixed methane-air flames. Similar observations were reported in atmospheric pressure flames by Stohr et al..[20-24] A recent review paper by Candel et al[16] presented a large body of work on the topic of instabilities in swirl-stabilized flames. However, as pointed out in the paper, the majority of this work is based on atmospheric pressure premixed gaseous flames. Introduction of a poly-disperse liquid spray results in stratification of fuel and air transported to the flame, leading to changes in the flame structure caused by the inhomogeneity in the mixture fraction. The uneven response of fuel and air to incident acoustic waves can alter the swirling flame characteristics. While some studies of non-premixed and partially premixed flames using liquid fuels have been conducted at atmospheric and moderate pressures,[25-29] more work on high pressure combustors is necessary to understand the mechanisms at work at operating conditions relevant to aviation gas turbines.

The present study aims to extend the body of work on LDI and other swirl stabilized combustors to a liquid-fueled, single-element model gas turbine combustor operating at a high chamber pressure (1 MPa). Self-excited dynamics are of specific interest. The objectives of the current paper are to assess the capability of the simulation to predict the measured dynamics behavior, and to identify and study the mechanisms that determine the combustion instabilities in the single-element LDI gas turbine combustor.

The paper is organized as follows. First an overview of the experimental design and the computational approach is presented. Experimental measurements are presented thereafter for two operating conditions with an inlet air temperature of 800K and equivalence ratios of 0.6 and 0.36. Results from the experiment and a large eddy simulation are compared in terms of high-frequency pressure fluctuation amplitudes and power spectra. It will be seen that the simulation can predict the measured pressure behavior fairly well at an equivalence ratio of 0.36, where the pressure oscillation amplitudes are fairly low. Hence, the results from the simulation at this condition are studied further in greater detail. An acoustically-open geometry is used to investigate the natural hydrodynamic modes present in the LDI combustor. Following this. an acoustically-closed geometry is used to identify the important instability mechanisms in LDI combustor. Dynamic Mode Decomposition (DMD) is used, first to identify the periodic dynamics in the LDI combustor, and second to establish interactions between the different physics. The paper concludes with an assessment of the simulations and recommendations for future work.

II. Comparisons of Experiment and Computations

A. Experiment Overview

The single-element LDI combustor design is based on achieving a self-excited axial mode combustion instability with a fundamental frequency between 300-400 Hz. Low-level amplitudes less than a few percent of mean pressure are desired, so that the spray formation process is not overly affected and the oscillations are still a fraction of the pressure drop through the subsonic venturi. The major dimensions of the combustor are determined at operating conditions tabulated in Table 1 based on a 1-D linearized Euler equation (LEE) solver.[30-32] The combustor operates at a mean chamber pressure of 1 MPa. The combustor uses liquid fuel (Jet-A/ FT-SPK) and heated air up to 800 K.

Table 1. Summary of design envelope and nominal operation parameters.

Fuel	Jet-A and FT-SPK
Inlet Air Temperature	650 – 800 K
Equivalence Ratio	0.37 - 0.7
Inlet Boundary Condition	Constant mass inflow from a choked orifice
Exit Boundary Condition	Choked nozzle
Diameter of combustor	50.8 mm
Diameter of air plenum	25.4 mm

A schematic of the LDI combustor is shown in Fig. 1. It comprises an air inlet section, air plenum, swirler-venturi-injector assembly, combustion chamber, and exit nozzle. Air, heated with an 80 kW electrical heater, enters the combustor through a slotted choked orifice plate, designed to minimize shock-induced unsteadiness. A converging-diverging subsonic venturi with an included angle of 90° at the inlet and outlet is located at the downstream end of the air plenum. The air mass flow rate is calculated across a sonic venturi with a known co-efficient of discharge. The pressure and temperature upstream of the orifice plate is monitored to maintain a constant air flow rate during the test. The length of the air plenum can be changed in discrete increments from 0.19 m to 0.56 m to tune the combustor dynamics to the target frequency and amplitude. A helical vane axial flow swirler with six vanes, each with a tip angle of 60º, is located at the end of the air plenum.

A hollow cone pressure swirl atomizer with a flow number of 1.32 is used to supply fuel to the combustor and is located at the end of the air plenum. A Coriolis flow meter (Micro Motion Coriolis ELITE, 0.1% accuracy) is used to measure the mass flow-rate of fuel. The fuel is sparged using nitrogen prior to testing to remove any dissolved air content from the fuel. The oxygen content in the fuel is monitored and ensured to be below 1% (by vol.) during tests to avoid coking in the feed lines in the combustor. The diameter of the combustion chamber is 50.8 mm and its length can be varied in discrete increments from 0.28 m to 1.08 m, similar to the air plenum. To approach an adiabatic wall boundary condition, thermal barrier coating (TBC - MCraly bond and Yttria stabilized Zirconia coating) is applied to the first 0.10 m of the combustion chamber and the diverging section of the venturi where the maximum heat release occurs. This provides better comparison with computational results where adiabatic wall boundary conditions are generally used for the combustor walls. The TBC also provides a thermal wall condition similar to the quartz tube used in tests requiring optical access. A choked nozzle at the end of the combustion chamber controls the chamber pressure at ~1 MPa and provides a well-defined downstream boundary condition.

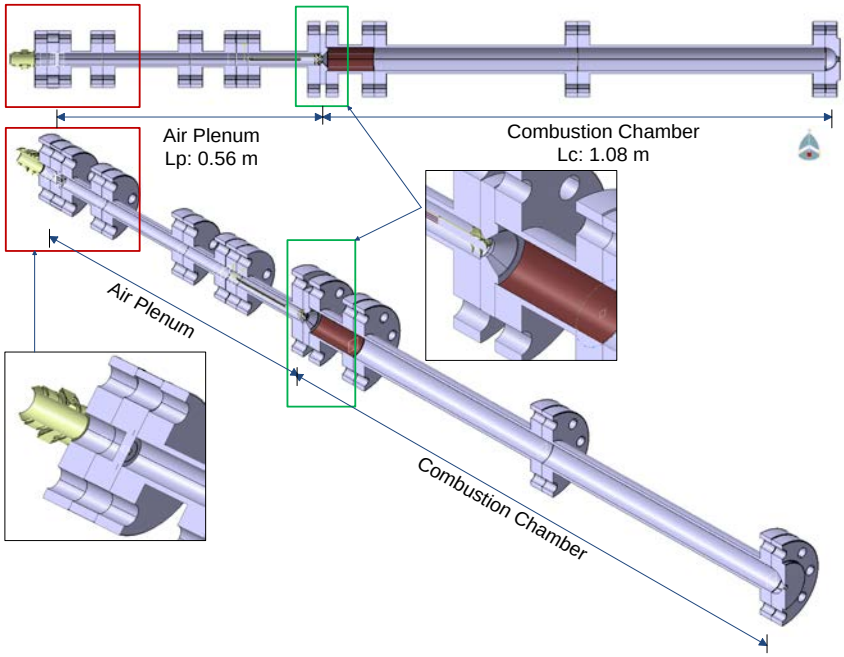

Figure 1. Schematic of the LDI combustor.

The combustor is instrumented with piezoresistive pressure transducers (Kulite WCT-312M-10/35/70 BARA) at multiple locations. The transducers are recessed from the combustor inner wall to avoid high thermal loading on the sensor element. The recess cavity is designed as a Helmholtz resonator with a resonant frequency that is much higher (~14 kHz) than frequencies of interest in the experiment. The transducers are located at six axial locations, three in the air plenum and three in the combustion chamber, as shown in Fig. 2. Two transducers are located at each axial location in the combustion chamber diametrically opposite to each other for identification of modes that are not purely longitudinal in nature. Data are collected from these transducers at 100 KHz. Temperature measurements are obtained using k-type thermocouples (Omega GKMQSS-062G) flush with the inner diameter of the combustor at the same axial locations as the pressure measurements. Feed system and combustor pressures are also obtained at a lower sampling rate (100 Hz– 2 kHz) using GE Sensing (UNIK 50E6 series; 0.04% accuracy) pressure transducers for controlling and monitoring combustor operating conditions.

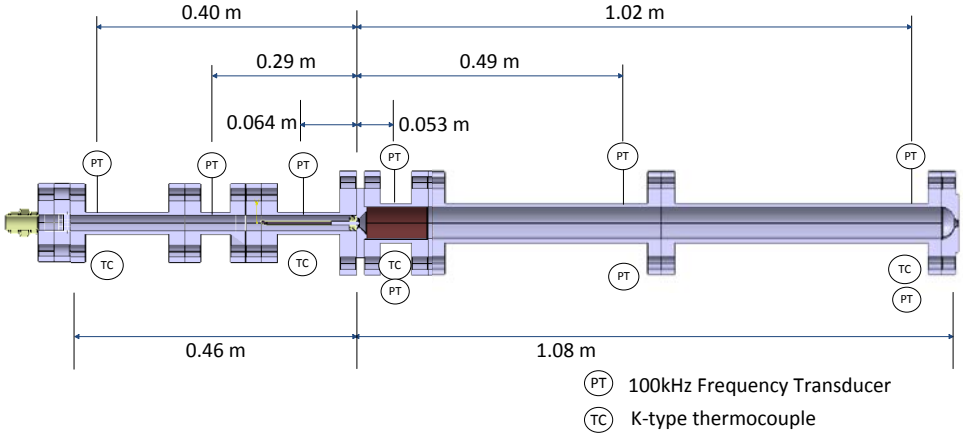

Figure 2. Location of pressure and temperature instrumentation on the combustor. A 3/8 wave air plenum and 1/2 wave combustion chamber configuration is shown.

The LDI combustor has been operated at a range of parameters with changes in geometry, operating condition, fuel nozzle location and fuel used. A summary of these parametric changes is provided in Table 2 below. The check marks in the second and third column of the table indicate that the particular geometry combination with corresponding air plenum configuration was tested, while cross marks indicate that the geometry was not tested. The lengths of the air plenum and combustion chamber are based on the calculated 1L (first longitudinal) mode-shape using LEE. Figure 3 shows a schematic depiction of different geometric configurations that have been tested.

Table 2. Summary of combustor configurations and operating conditions.

Geometric Parameters			Operational parameters	
Air plenum	Combustion chamber			
	1/4 wave (short combustor)	1/2 wave (long combustor)	ϕ	Tair (K)
1/4 wave	✓	✓	0.7 - lean blow-out (~0.37)	650
3/8 wave	×	✓		700
1/2 wave	✓	✓		750
Full wave	×	✓		800

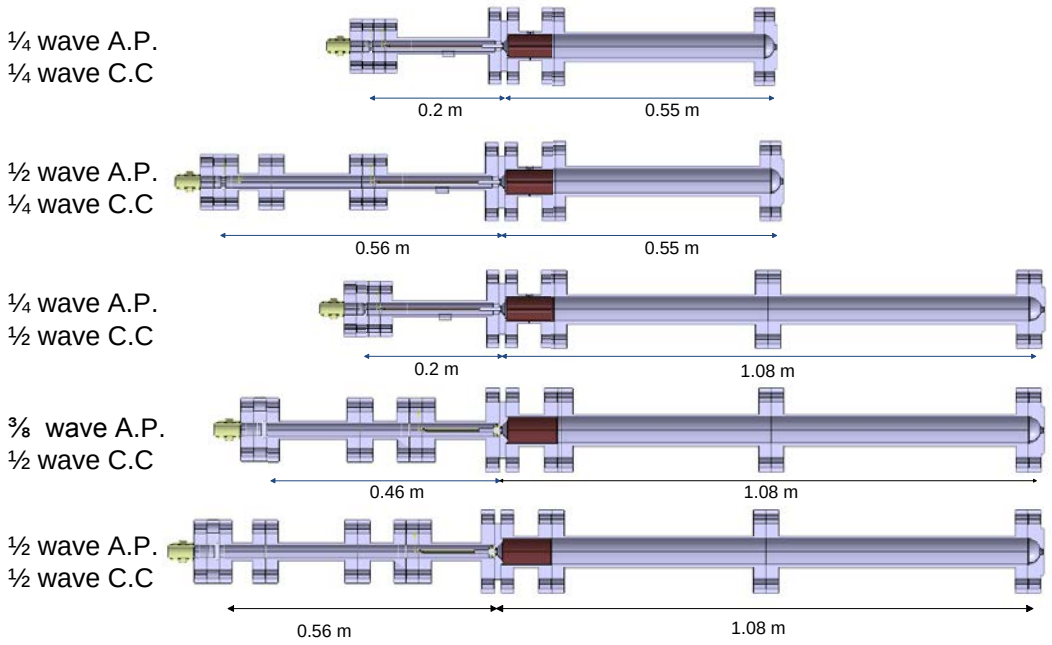

Figure 3. Geometric configurations of the LDI combustor.

Results for all tests are summarized in Fig. 4. A preference for the instability to be driven at higher acoustic modes (4L or 5L) between 1,000 and 2,000Hz is clearly indicated, while it should be noted the fundamental frequency of the combustor is designed to be 300-400Hz (1L) for a 1/2 wave chamber. Even with the shortest combustor (1/4 wave), response at that frequency is quite significant. This observation indicates the possible couplings between acoustic field and other important physics, including the natural flow dynamics present in the LDI combustor. Moreover, strong oscillations around 7 kHz are also present in all test configurations, which can be produced by either even higher harmonics of acoustic modes or other hydrodynamic modes.

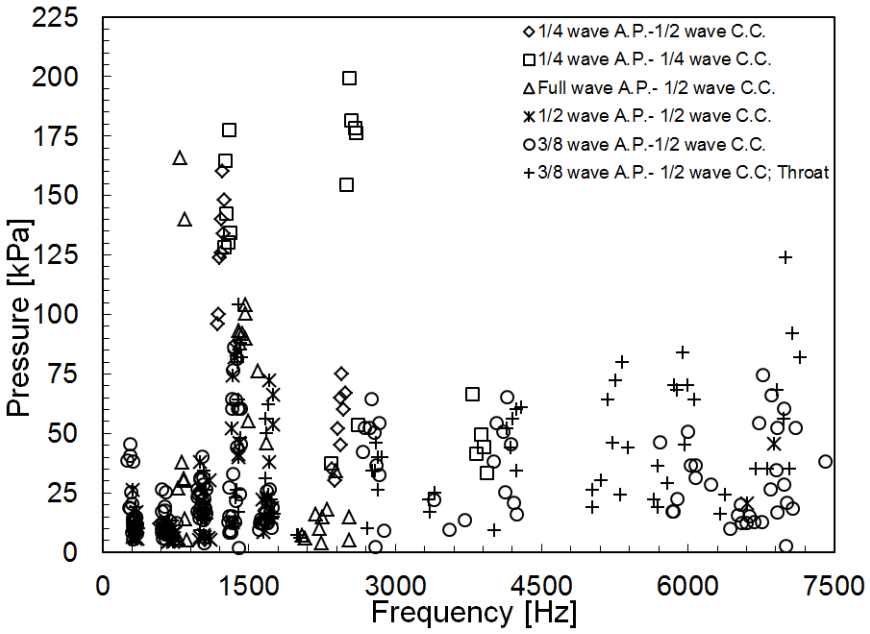

Figure 4. Summary of pressure oscillation amplitudes (peak-to-peak) as a function of frequency for all tests.

In addition, the effect of the fuel injector location with respect to the throat of the converging-diverging venturi was measured for the 3/8 wave air plenum and 1/2 wave combustion chamber configuration. The configuration with the fuel nozzle at the throat was more unstable than the configuration with fuel nozzle upstream (2.6 mm) of the throat. Details of experimental parametric studies in LDI combustor can be found in Ref. 33.

B. Computational Approach

The present simulations are based on time-accurate solutions of the Navier-Stokes, energy and species equations.[34-38] The numerical scheme is second order accurate in both time and space and uses an implicit formulation allowing for the use of high-aspect ratio grids near the wall. A dual-time formulation is used to eliminate approximate-factorization and linearization errors. Turbulence is modeled using a hybrid RANS/LES formulation [39,40] where the near wall region is modeled using a two-equation k-ω model.[41,42] Combustion is accounted for using a simplified two-step, five-species global reduced mechanism[43] with laminar kinetics. Global reactions allow for the coupling between pressure and heat release while also minimizing the number of species that must be retained.

$$2\mathbf{C_{12}H_{23}} + 35\mathbf{O_2} \longrightarrow 24\mathbf{CO} + 23\mathbf{H_2O}$$
$$2\mathbf{CO} + \mathbf{O_2} \longleftrightarrow 2\mathbf{CO_2}$$

Modeling of direct injection sprays for gas turbine engines has been developed for combustion dynamics problems. This method combines sub-models for atomizing, vaporizing and reacting sprays. Key physical events considered in the present model include the free-surface jet in the atomizer, primary and secondary breakup, droplet vaporization, mixing and burning. The models are implemented within a Lagrangian-Eulerian framework, where the droplet phase is described by Lagrangian dynamics and the vaporized fuel is input as a source term along with associated momentum and energy terms in the Eulerian gas-phase equations. Yoon et al.[44] summarized computational investigations of fuel spray modeling effects on combustion instability predictions, which indicates the significant role of fuel spray modeling.

Currently, there are three major submodels for atomization as described by Yoon et al.[45]: atomizer free surface flow, primary, and secondary atomization models. Preliminary computational studies using these three submodels have been done by Huang et al.[46] The first submodel is the atomizer free surface flow. Independent calculation of the free surface internal flow in the atomizer is used to provide the spray injection conditions of the Lagrangian spray particles. Ashraf and Jog's numerical model [47] is employed for the present study. This model directly solves the two-phase flow using the Eulerian Volume-Of-Fluid Method and provides the spray angle, liquid sheet thickness, and velocity. This information is delivered to the second sub-model, i.e., the primary atomization model. Primary atomization is described by the linear stability analysis of the liquid sheet proposed by Senecal et al. [48] Using the liquid sheet thickness and velocity, the most unstable wave length and maximum growth rate are determined by a dispersion relation derived from linear stability theory, and ligament and drop sizes disintegrated from the liquid sheet are then calculated. Lagrangian drops produced by the primary atomization then undergo the secondary atomization process, which is in turn represented by the third sub-model. During secondary atomization, the drops may be broken up by several kinds of modes. The secondary atomization model used here covers the full Weber number range typically encountered in gas turbine combustors. Depending on the local Weber number, a secondary atomization model based on the Taylor Analogy Breakup (TAB), [49] Kelvin Helmholtz (KH), or Rayleigh-Taylor (RT) models is applied. [50-52]

The computational geometries are shown in Fig. 5. The open geometry is used to explore the natural hydrodynamic modes that arise from the swirling flow going through the converging-diverging venturi section. A weak acoustic field is set up by using the open-end so that the natural hydrodynamic modes can be seen. The closed geometry is modeled based on the experimental configuration shown in Fig. 1 with all important details (A, inlet choked slots; B, swirler; and C, choked exit nozzle) to ensure direct comparisons between experimental measurements and simulation results. A time step of 0.5 μs is used and simulations are typically run for 200 ms to provide sufficient cycles for analysis. All computations are three-dimensional and contain approximately 5 million grid points.

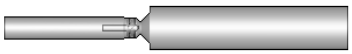

Open Geometry

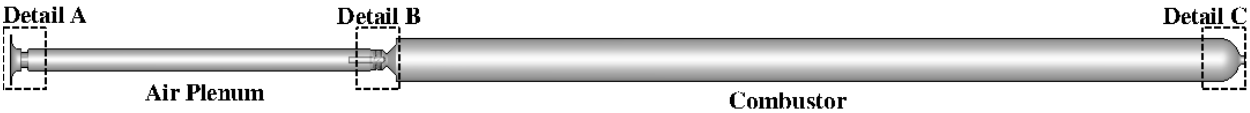

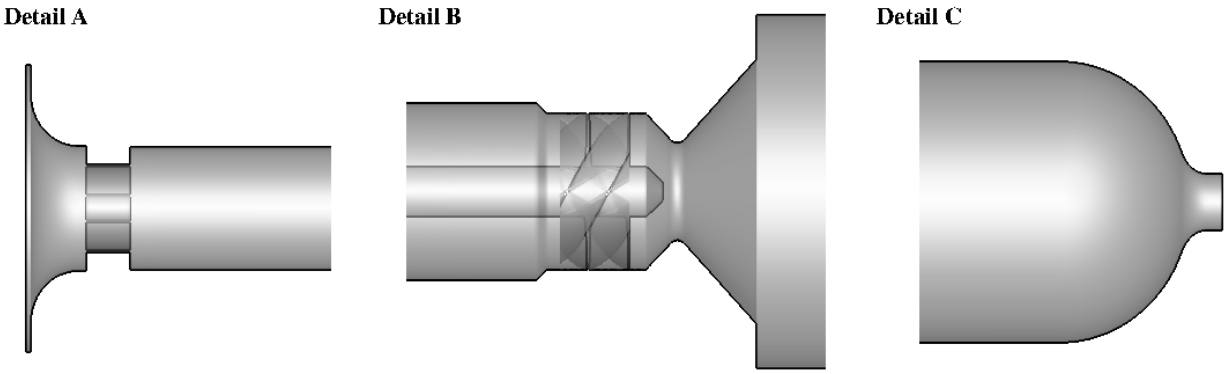

Closed Geometry

Figure 5. Schematic drawing of computational geometries.

C. Comparisons of Pressure Signals

Figures 6 and 7 below show the comparisons of pressure signal between measurement and prediction at high and low equivalence ratio, respectively. The pressure signals have been high-pass filtered and taken at the same location near the combustor head section for both experiment and simulation.

For the high equivalence ratio (Fig. 6), a peak-to-peak pressure fluctuation amplitude around 0.1 MPa can be seen in both experiment and simulation. Also, the 4L and 8L acoustic modes can be clearly identified in the power spectral density plots. However, the multiple modes between 6 and 8 kHz (identified in most test configurations - see Fig. 4) cannot be fully captured in the simulations.

For the low equivalence ratio (Fig. 7), lower peak-to-peak pressure amplitude (around 30 to 40kPa) can be observed in both experiment and simulation. The 1L acoustic mode is more distinguishable in the PSD plots than in the high equivalence ratio case. The dominant acoustic modes have been shifted to higher 5L and 6L acoustic modes. In the experiment, an even distribution in the PSD can be observed for lower frequencies (1L to 4L), while in the simulation, a collapse in PSD of 2L to 4L modes can be found. The simulation under-predicts both the PSD and the frequencies of responses higher than 6 kHz while, in the experiment, the high frequency peak lies around 7 kHz and has comparable PSD as 1L.

Overall, the simulations predict reasonable pressure amplitudes and captures the dominant acoustic frequencies measured in the experiments for both high and low equivalence ratio, but it does not capture the high frequency modes between 6 and 8 kHz. Since the low equivalence ratio simulation provides better general agreement with measurements, and because the behavior at lower amplitudes are of more practical interest, more detailed investigation of the combustion dynamics at Φ = 0.36 are presented below.

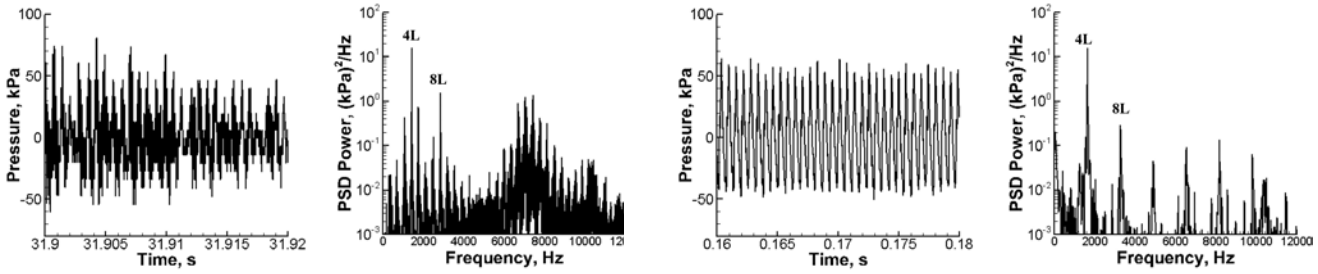

Experiment Simulation

Figure 6. Comparison of high pass filtered pressure data and power spectral density (PSD) for Φ = 0.6 T_{air} = 800K between experiment (left) and simulation (right).

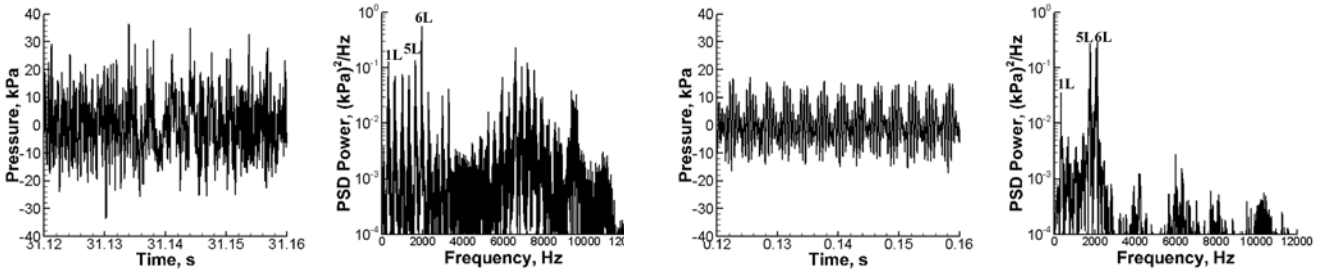

Experiment Simulation

Figure 7. Comparison of high pass filtered pressure data and power spectral density (PSD) for Φ = 0.36 T_{air} = 800K between experiment (left) and simulation (right).

III. Identification of Instability Mechanisms

Results from the simulation at low equivalence ratio (Φ = 0.36) are examined in detail in this section with the objective of identifying the underlying instability mechanisms. Open geometry simulation results are presented first to illustrate the natural hydrodynamic modes that exist in the single LDI combustor, in the absence of strong acoustic forcing. The correlations between hydrodynamic modes and combustor acoustic modes are established based on Dynamic Mode Decomposition (DMD) analysis of the open geometry simulation. Cycle studies are performed next based on closed geometry simulation results to identify the key processes that lead to combustion instabilities in the LDI combustor. The major findings and observations from the simulations can be summarized as follows:

1. The presence of a natural hydrodynamic mode – identified here as the Vortex Bubble Breakdown (VBB) mode – and its coupling with the chamber acoustic modes leads to instabilities at higher acoustic modes.

2. Partial coupling between 1L acoustic and the first VBB mode (VBB1) can possibly modulate the amplitude of pressure oscillations.

3. Another important hydrodynamic mode, the Precessing Vortex Core (PVC), is also be identified through DMD analysis, and appears to correspond to the high frequency content observed in the pressure power spectra.

4. The potential nonlinear coupling between the dominant acoustic modes (5L) and the PVC hydrodynamic mode may enhance intermediate frequencies around 4 kHz.

A. Open Geometry Simulation

The open geometry simulation is conducted at the baseline equivalence ratio (Φ = 0.36), air temperature (T_{air} = 800K) and mean chamber pressure (p_{back} = 1MPa) to ensure that both spray and combustion are subject to similar conditions as in the closed geometry simulation. Examination of the power spectral densities of the pressure oscillations in the open-geometry simulation reveals that the acoustic perturbations are small and the dominant responses are tied to the natural hydrodynamic modes of the injector. Figure 8 shows evidence of the so-called vortex bubble breakdown (VBB) mode and its cyclic behavior over one period. The VBB mode in this configuration has a natural frequency of 575Hz. A contour line of zero axial velocity (U = 0) has been selected in each snapshot to visualize the mode in the region near the combustor head section. Flow inside the bubble (white line) travels upstream and flow outside goes downstream, triggering a pair of counter rotating vortices indicated by the white arrows in the first snapshot (top velocity contour). The swirling motion introduced by the air swirler upstream of the venturi produces a clockwise rotation of the flow in the azimuthal direction, as seen in the cross sectional view near the exit of the venturi section.

The influence of the VBB process can be investigated by looking at the fuel mass fraction and heat release contours at the bottom of each snapshot. At t = 0T/4, the vortex bubble is strong and compact. Starting from t = 0T/4 to t = T/4, it grows and stretches downstream. During the growth, the reverse flow has been amplified, which anchors the fuel distributed within the diverging section of the venturi. As a result, the heat release distribution is compressed in the diverging section. The stretching of the vortex bubble is greatest at t = T/4 beyond which it starts to break down. The bubble becomes weak at t = 2T/4, and the regions of high fuel concentration and heat release move further downstream into the combustor. As the bubble continues to breakdown (at t = 3T/4), it is compressed to its minimum size, at which point it entrains more fuel into the center of combustor and the heat release becomes even more stretched out.

The use of Dynamic Mode Decomposition (DMD) provides clearer insight into the dynamic patterns of the quantities of interest. The DMD procedure is similar to Proper Orthogonal Decomposition (POD) but whereas POD typically has multiple frequencies associated with each mode, each DMD mode only contains a single frequency.[53] Comparisons between the DMD and POD analyses applied to axial combustion instabilities by Huang et al.[54] has led to the conclusion that the underlying physics can be more efficiently understood with DMD, especially when there are strong instabilities present. Here, the DMD is performed to investigate the fluctuating parts of quantities shown in Fig. 8. The frequency spectra of the VBB mode, the fuel mass fraction, and the heat release modes are plotted in Fig. 9, which clearly show the coupled behavior of the three quantities. The fundamental frequency is around 575Hz, which corresponds to the first VBB mode (VBB1). We also note that the DMD spectrum does not show any significant acoustic mode content in the chamber for this open geometry simulation. We will contrast this later with the spectrum corresponding to the closed geometry simulation.

The reconstructed DMD response of VBB1 is shown in Fig. 10 to more clearly illustrate the hydrodynamic patterns and its coupling with fuel mass fraction and heat release. Two representative time instants were selected. Snapshots at left show the VBB responses when the reverse flow is highest, and when the fuel and heat release is more concentrated in the diverging section of the venturi. Snapshots on the right-side show the responses as the VBB breaks down (at t = 3T/4). The axial velocity increases, more fuel is brought downstream into the combustor, and heat release stretches downstream as well. The clockwise rotation of flow in the azimuthal direction can also be visualized by the contours in the cross-sectional view.

The higher VBB modes are shown in Fig. 11. With increasing frequency, the higher modes show more spatial variations in the azimuthal direction (see cross-sectional view), and a concomitant reduction in the scale of vortices.

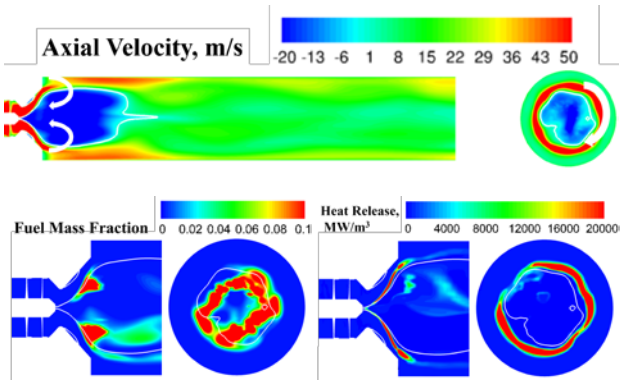

t = 0T/4

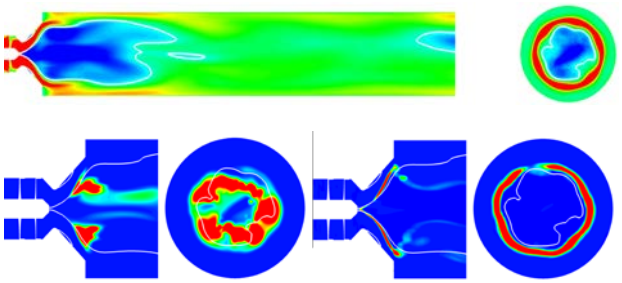

t = 1T/4

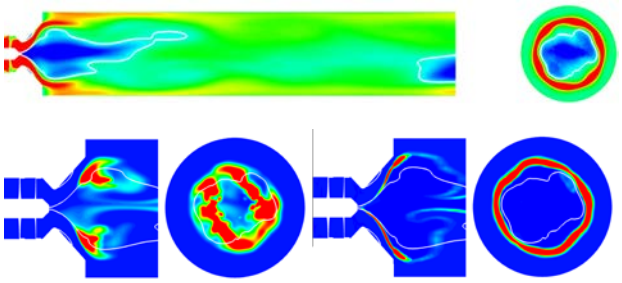

t = 2T/4

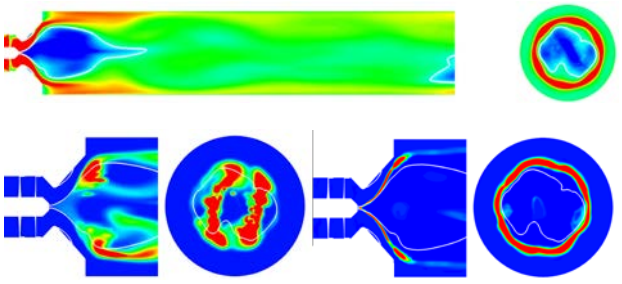

t = 3T/4

Figure 8. Time history of open geometry simulation for Φ = 0.36 T_{air} = 800K in one cycle of period (left: axial velocity; middle: fuel mass fraction; right: heat release; white line: contour line of U = 0; cross section view is selected near the exit of venturi).

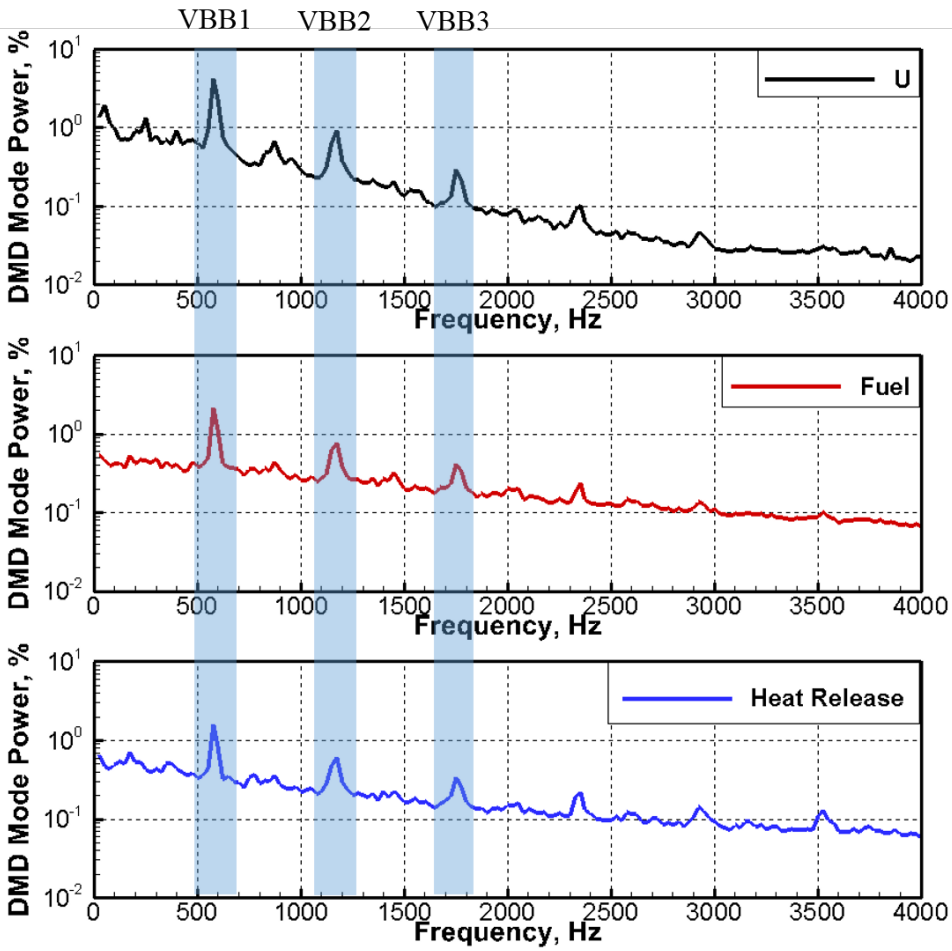

Figure 9. DMD frequency spectrum of open geometry simulation for Φ = 0.36 T_{air} = 800K (top: axial velocity; middle: fuel mass fraction; bottom: heat release).

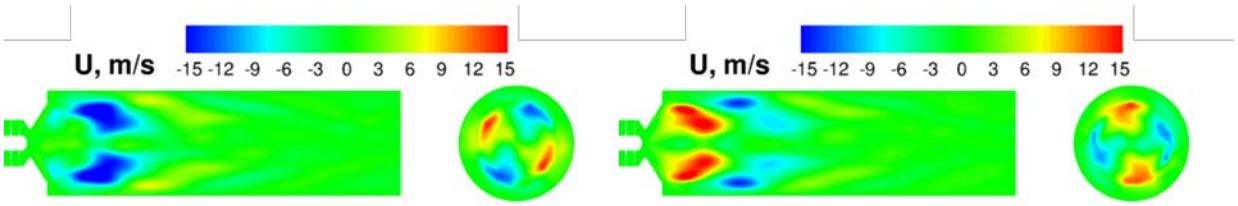

Axial Velocity

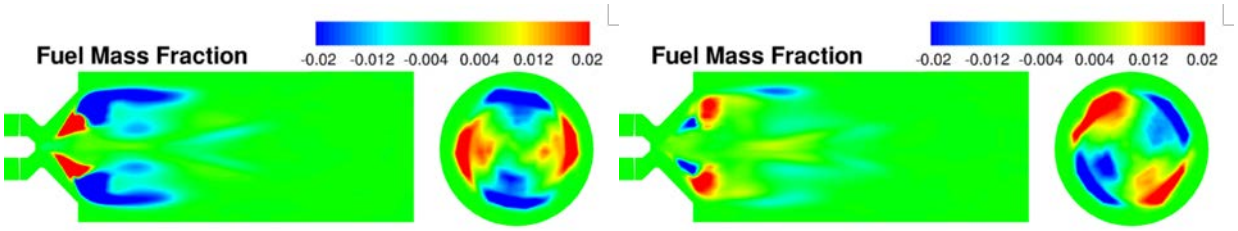

Fuel Mass Fraction

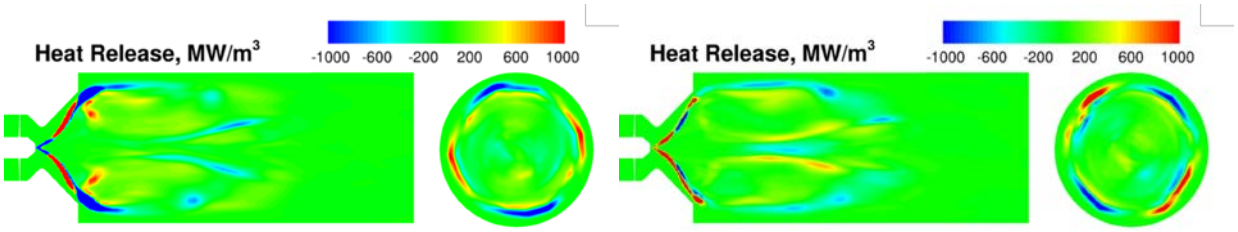

Heat Release

Figure 10. Reconstructed DMD responses at VBB1 for open geometry simulation for Φ = 0.36 T_{air} = 800K at two representative time instants (left: growth of VBB; right: breakdown of VBB).

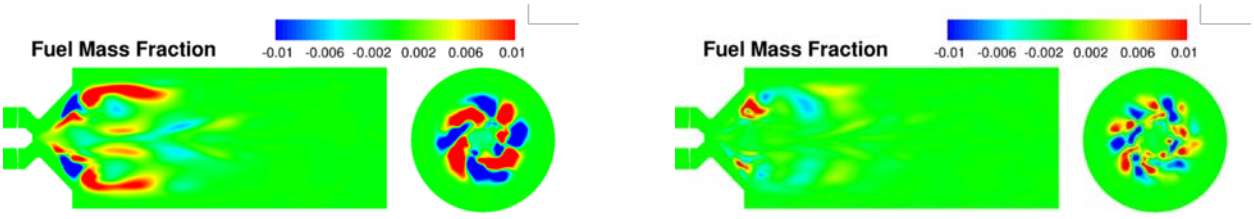

VBB2 VBB3

Figure 11. Higher harmonics of VBB modes reconstructed from DMD analysis for open geometry simulation for Φ = 0.36 T_{air} = 800K (fuel mass fraction only).

The frequencies of the VBB modes calculated from the open geometry simulation and the acoustic modes calculated from the closed geometry simulation are summarized in Table 3. It should be noted that the frequency of

VBB modes summarized in Table 3 are weakly influenced by the acoustic field and it could be expected that stronger acoustic interactions in a closed chamber may cause a shift in the behavior of the VBB modes and hence a shift in the behavior of fuel distribution and heat release. These details will be discussed in greater detail in the following section that considers the closed geometry simulation results.

VBB Mode	Frequency, Hz
1st Harmonic	575
2nd Harmonic	1175
3rd Harmonic	1750
4th Harmonic	2350
Acoustic Mode	**Frequency, Hz**
1st Harmonic	330
2nd Harmonic	660
3rd Harmonic	990
4th Harmonic	1320
5th Harmonic	1650
6th Harmonic	1980

Table 3. Summary of frequencies of hydrodynamic modes and acoustic modes identified in LDI combustor using open and close geometry simulation respectively.

B. Closed Geometry Simulation

In this section, we examine the important instability mechanisms observed in the LDI combustor by considering an analysis of the results of an acoustic cycle corresponding to the closed geometry simulations. This case corresponds to the PSD results in Fig. 7, which are dominated by 5L and 6L acoustic response. Two mechanisms are noted: first, enhanced vaporization of fuel droplets due to the incoming compression wave; and second, interactions between the compression wave and the VBB that triggers enhanced mixing. In addition, DMD analysis is used to elucidate the other important physical interactions in LDI combustor. The incomplete coupling between VBB1 mode and the 1L acoustic mode introduces a modulation of the pressure oscillation amplitude around the 1L frequency. Next, a second hydrodynamic mode, the so-called Precessing Vortex Core (PVC), is identified and speculated to be the source of high frequency pressure oscillations between 6 and 8 kHz observed in the PSD plots (Fig. 7). Finally, the potential for nonlinear interactions between the dominant acoustic modes (5L and 6L) and the PVC mode is also discussed.

a. Cycle Analysis

Figure 12 shows a pressure-time trace taken just downstream of the combustor dump plane from the simulations. Two dominant acoustic cycles can be identified in Fig. 12. First, the pressure fluctuates mainly at the 5L and 6L frequencies. Second, modulations in the pressure amplitude can be observed at the 1L frequency. Figure 12 also highlights the specific acoustic cycle that will be examined in detail in this section. This represents a single 6L cycle as shown by the dashed box on the top-half of Fig. 12. Five time instants are selected to examine the physics as shown on the bottom-half of Fig. 12. In addition, the axial and azimuthal velocity signals are plotted at the same location to help understand the interactions between fluid dynamics and acoustics.

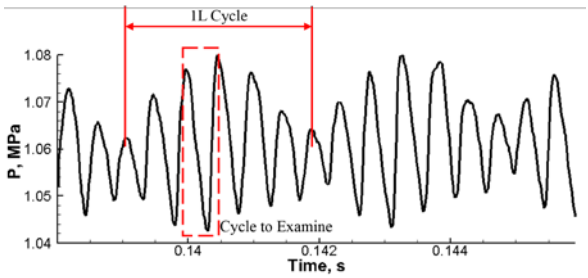

(a) Overview of Pressure Cycle

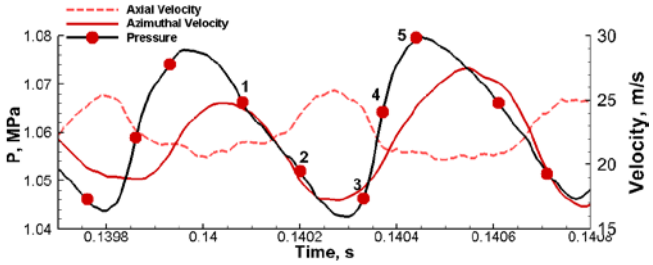

(b) Acoustic Cycle for examination

Figure 12. Acoustic cycles defined based on dominant longitudinal frequencies.

Figures 13 and 14 show a series of plots for the five points in the cycle marked in Fig. 12 (b). Figure 13 limits the side-view of pressure contours to the first 25% of combustor length to focus on the dominant acoustic mode. The isosurface of zero axial velocity is overlapped and colored by pressure on the plots to visualize the vortex breakdown bubble. The cross-sectional view is selected near the exit of venturi to visualize the three-dimensional effects in the combustor. Figure 14 shows the behavior of the spray and combustion in the diverging section of the venturi and just downstream of the dump plane, where most of their dynamics happen. A white isoline of U = 0 is attached in each subplot to locate the vortex breakdown bubble. Fuel mass fraction contours are shown on the left with the fuel vaporization rate overlapped and colored in grey scale. Heat release contours are shown on the right with the fuel droplets sized by the radius and colored by the Weber number. Contour lines of fuel mass fraction are attached on the heat release contours in the cross-sectional views. The cross-sectional views are selected at the same location as those used in Fig. 13.

Starting at Time 1, the pressure in the combustor head section is decreasing from its maximum value (acoustic expansion process at combustor head) and the axial velocity starts to increase. The acoustic wave is traveling downstream and a well-defined spray cone angle can be identified (~64°). Because pressure is relatively high at Time 1, a high Weber number is observed from the color on the spray drops. The large drops are relatively unstable, and they are broken up into small drops in the diverging section. The high pressure wave compresses the vapors, increases gas-phase density and thereby increases fuel spray vaporization so that fuel mass fraction level increases. During the expansion of acoustic wave, the axial velocity increases and vortex breakdown bubble gets compressed. Similar to the observations in Fig. 8, gaseous fuel follows the compressed bubble, extends into the combustor, and results in a more distributed heat release that stretches into the combustor as well.

At Time 2, the Weber number decreases with the decreasing pressure, less secondary atomization occurs, and a higher number of larger drops are left in the diverging section. Vaporization is slower compared with Time 1, causing a reduction in the level of gaseous fuel and heat release.

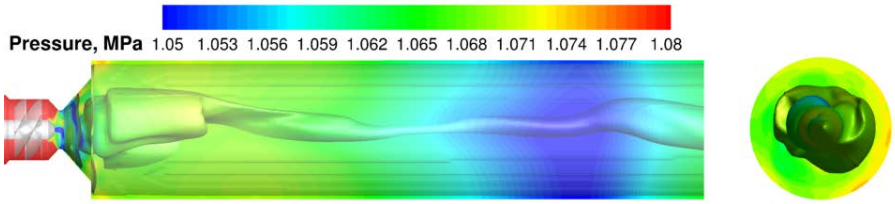

(a) Time 1

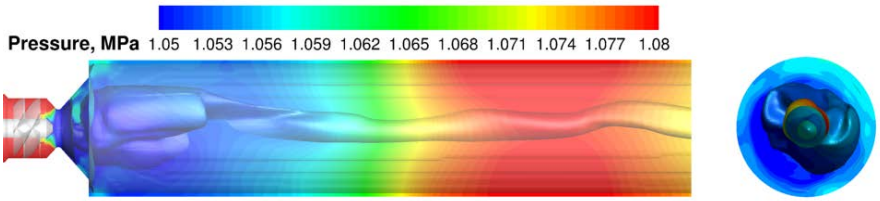

(b) Time 2

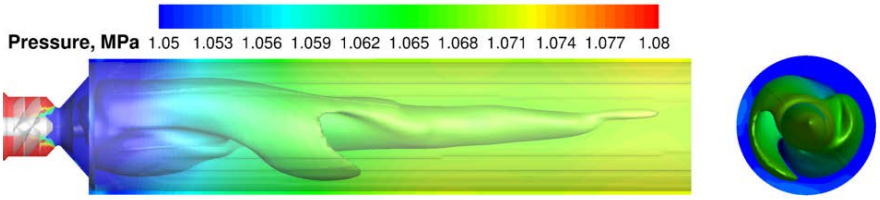

(c) Time 3

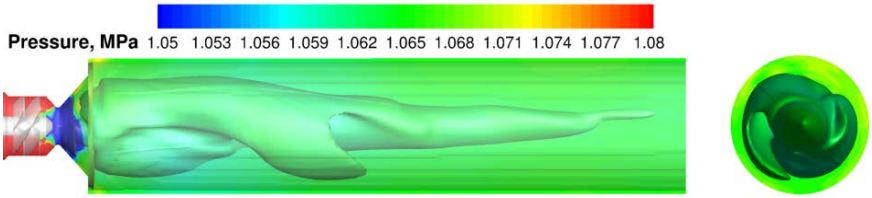

(d) Time 4

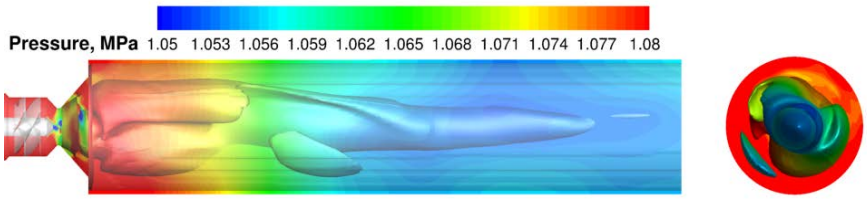

(e) Time 5

Figure 13. Time history of acoustic field in closed geometry simulation for Φ = 0.36 T_{air} = 800K in one 6L cycle (The isosurface represents the Vortex Breakdown Bubble (U=0) and colored by pressure; cross section view is selected 1mm upstream to the exit of venturi).

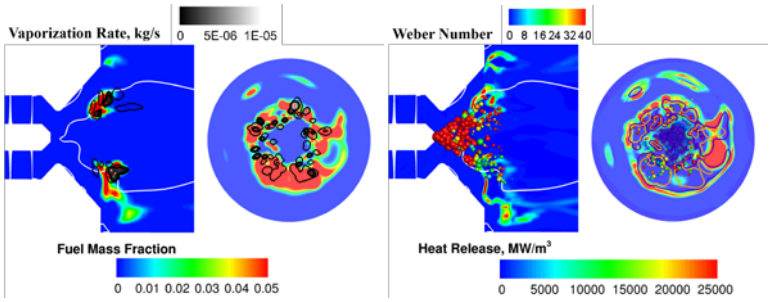

(a) Time 1

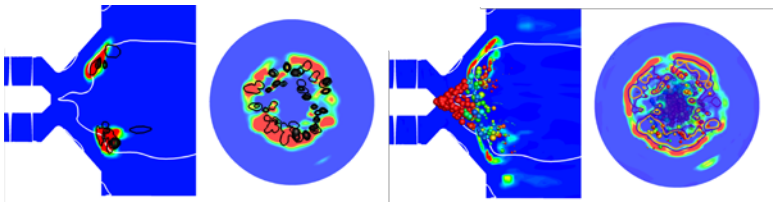

(b) Time 2

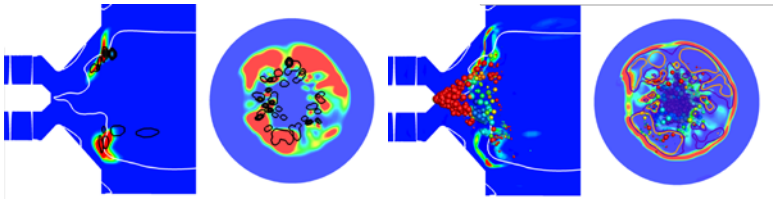

(c) Time 3

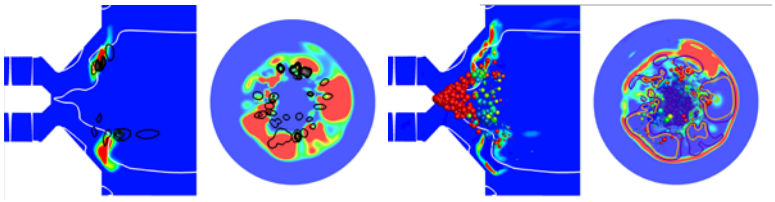

(d) Time 4

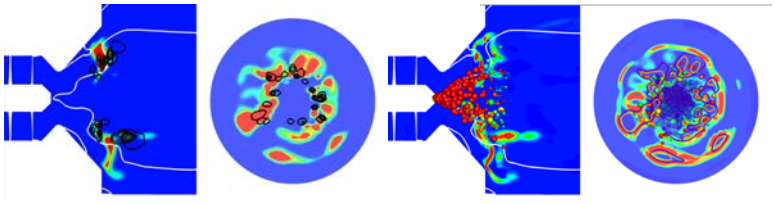

(e) Time 5

Figure 14. Time history of combustion and spray characteristics in closed geometry simulation for Φ = 0.36 T_{air} = 800K in one 6L cycle (left - fuel mass fraction and fuel vaporization rate; right - heat release with spray drops overlapped, sized by radius and colored by Weber number; white line: contour line of U = 0; cross section view is selected near the exit of venturi).

As we move from Time 2 to Time 3, the local pressure field transfers from an expansion to a compression process. Pressure starts to increase from its minimum value and the axial velocity starts to decrease. As pressure increases, the Weber number becomes higher, and smaller drops are generated in the converging section due to the secondary atomization models. Due to the enhanced vaporization from the compression, more gaseous fuel is produced from those small drops. The vortex breakdown bubble grows in this period due to the decrease in the axial velocity. As discussed in Fig. 8, as the VBB is growing, the amplified reverse flow restricts the fuel flow out of the diverging section, which in turn makes the flame in the acoustic compression phase more compact than in the expansion phase.

As the cycle steps from Time 3 to 4, acoustic compression becomes even stronger and pressure increases rapidly (Fig. 12). Drop breakup and fuel vaporization are enhanced and gaseous fuel is accumulated during the first half of acoustic compression process. The vortex breakdown bubble keeps growing and pushes the accumulated gaseous fuel further into the diverging section to mix and react with incoming swirling air. The increase in azimuthal velocity with pressure can be observed in Fig. 12. The acceleration of the swirling flow further enhances the mixing between fuel and air, which in turn leads to an increase in the heat release from Time 3 to Time 4.

The cycle completes at Time 5 when the pressure reaches its maximum value. The azimuthal velocity also increases to nearly its maximum. This indicates a continuous acceleration of swirling flows, which mixes more fuel with air, generating more heat release. The further enhancement of mixing and combustion from Time 4 to 5 keeps consuming the fuel so that less fuel exists in the diverging section at Time 5 than at Time 4. As the pressure peaks at Time 5, the vortex bubble starts to break down and gets compressed as it steps into a new cycle.

From the examination of the cycle described above, the acoustic field plays an important role in driving the VBB through the acoustic velocity field. Breakdown of the VBB happens during the period of acoustic expansion, while the growth of VBB occurs during the acoustic compression. During the breakdown, more fuel is brought downstream into the combustor away from air flow. With less mixing between fuel and air, the heat release level becomes lower and more distributed spatially. During the VBB growth, strong reversing flow pushes more fuel into the diverging section that can be mixed with incoming air. Also, the accelerated swirling motion in the third direction helps further enhance the fuel oxidizer mixing and generate more heat release in the combustor.

b. DMD Analysis

DMD analysis of the pressure, fuel mass fraction, and heat release modes from the closed geometry simulation is presented next. The DMD frequency spectrum is shown in Fig. 15. The spectrum of pressure is similar to the PSD plot in Fig. 7, showing the dominance of the 5L and 6L modes. Significant coupling with these acoustic modes is evident by the corresponding modes in the fuel mass fraction and heat release at the same frequencies. The spectra also show very strong modes of fuel mass fraction and heat release at about 4.5 kHz, which is not directly coupled to a strong acoustic mode. It should also be pointed out that the results are in contrast with the corresponding DMD spectrum for the open geometry shown in Fig. 11. An examination of the modes at the frequencies highlighted in Fig. 15 is provided next.

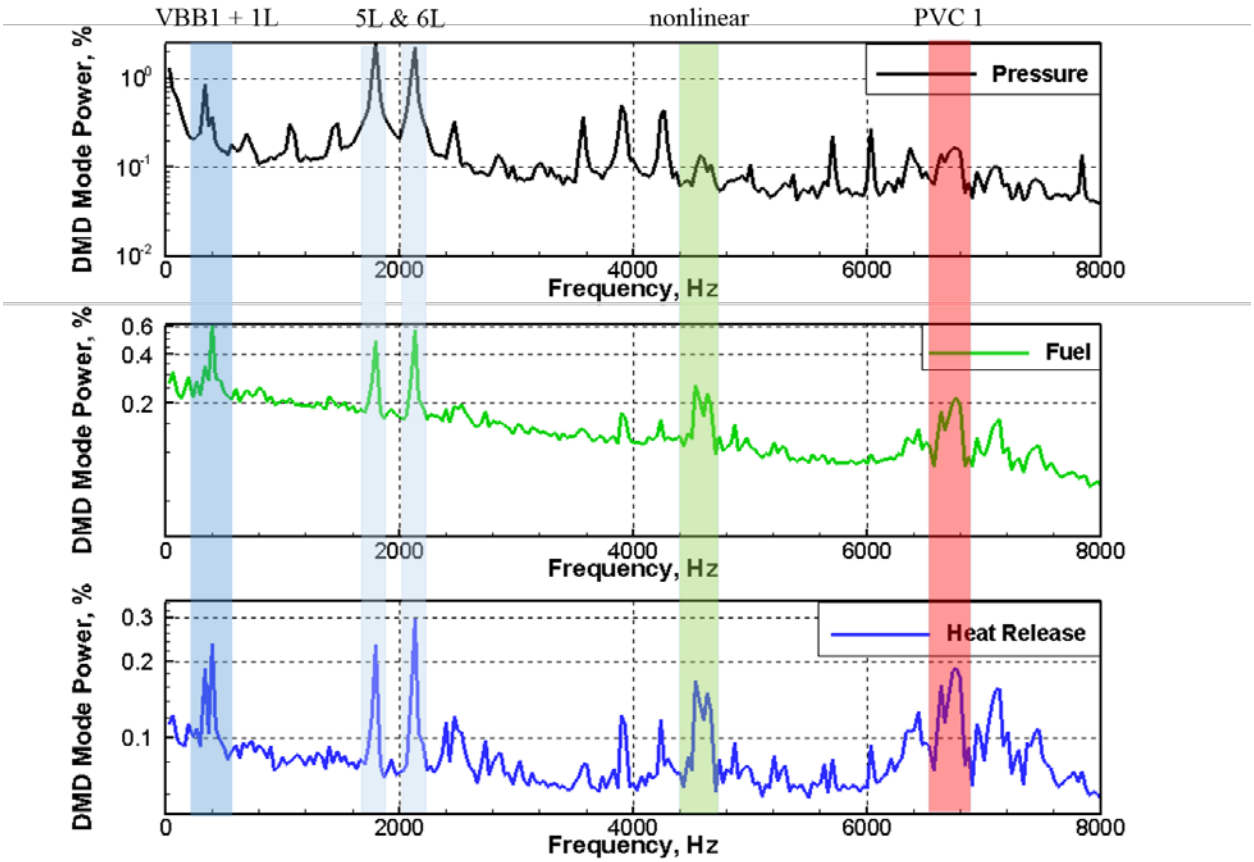

Figure 15. DMD frequency spectrum of closed geometry simulation for Φ = 0.36 T_{air} = 800K (top: pressure; middle: fuel mass fraction; bottom: heat release).

Starting from the responses at the most dominant acoustic frequencies (5L and 6L), and because of the similarity in the mode shapes, only a discussion of the 5L mode is included here. The major physics and coupling phenomena at these frequencies were discussed in the cycle analysis section. The reconstructed DMD responses help to extract specific mode shapes for the key physical quantities. Representative DMD responses for the 5L mode of the fuel mass fraction and heat release fluctuations are shown in Fig. 16. The spatial distributions of both modes are fairly uniform in the azimuthal direction with a ring-like structure in the cross-sectional views, indicating the strong driving effect of the one-dimensional axial acoustic field. The heat release fluctuations closely follow the variations in fuel mass fraction. Variations in the radial direction are seen in both modes, but are most apparent in the heat release mode and arise due to the axial velocity distributions of the VBB mode. As shown in Fig. 8, a strong reverse flow sits in the center region of combustor surrounded by a positive axial flow. The reversing flow pushes fuel back towards the injector, while the outside flow convects the fuel downstream along the combustor wall.

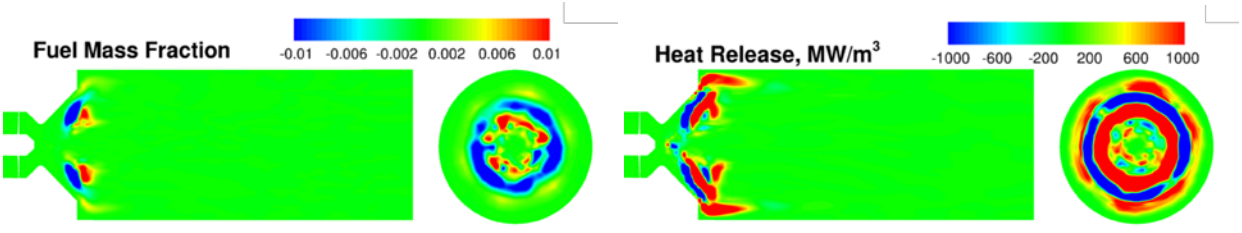

Figure 16. Representative reconstructed DMD responses at 5L for closed geometry simulation for Φ = 0.36 T_{air} = 800K (fluctuations of left: fuel mass fraction; right: heat release).

The DMD responses in the low frequency region are also interesting. In the open geometry simulation, with minimal acoustic influence, the vortex bubble breakdown is dominant at a fundamental frequency of 575 Hz. Here in the closed geometry simulation, double peaks in heat release are observed at the highlighted region (VBB1 + 1L). The 1L acoustic mode is around 330 Hz and the VBB1 mode is about 400Hz. The representative DMD responses of the fuel mass fraction and heat release fluctuations at the two frequencies are shown in Fig. 17. Although the difference in frequency is small (~70 Hz), the responses are seen to be very different. The similarity between the 1L and 5L results can be seen by comparing Figs. 16 and 17 (top). As mentioned above, longitudinal acoustic modes drive the fuel and heat release with little azimuthal variation. However, the modal responses at the VBB1 frequency (400Hz) show distinct azimuthal variations, the mode shapes of which are comparable to those in Fig. 10. A swirling motion is clearly indicated, and with the inclusion of the acoustic field, the distributions of fuel and heat release are seen to be more restricted within the diverging section and stretch to a lesser extent into the combustor (compared to Fig. 10).

In addition, as mentioned at the end of part A, the presence of the acoustic field alters the VBB frequencies from 575 to 400 Hz. Table 4 shows this effect by summarizing the important VBB and acoustic frequencies. Compare the VBB mode frequencies with those corresponding to the open geometry given in Table 3. The closed geometry results indicate a close coupling between the VBB4 and the 5L acoustic modes, and between the VBB5 and the 6L acoustic modes. In fact, these couplings may help explain the dominance of the 5L and 6L modes for this case as seen in the pressure spectra in Fig. 7. For low frequencies, the presence of two distinct modes (1L and VBB1) also helps explain the amplitude modulations at the 1L frequency observed in Fig. 12(a). We note, however, the 70 Hz (21% of 1L) frequency difference provides a less direct coupling between the 1L and VBB1 modes than the higher modes which drive the dominant response.

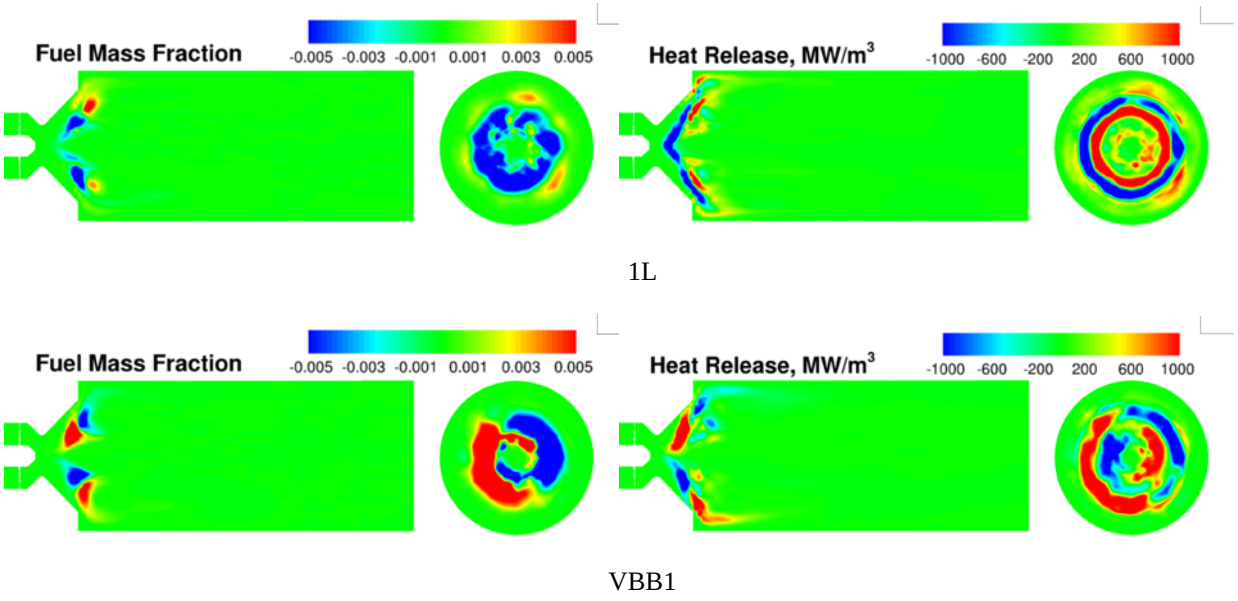

Figure 17. Representative reconstructed DMD responses at 1L (top) and VBB1 (bottom) frequencies for closed geometry simulation for $\Phi = 0.36$ $T_{air} =$ 800K (fluctuations of left: fuel mass fraction; right: heat release).

VBB Mode	Frequency, Hz
VBB1	400
VBB2	800
VBB3	1200
VBB4	1600
VBB5	2000
Acoustic Mode	**Frequency, Hz**
1L	330
2L	660
3L	990
4L	1320
5L	1650
6L	1980

Table 4. Summary of frequencies of hydrodynamic modes and acoustic modes identified in LDI combustor using closed geometry simulation.

In the high frequency region (>5 kHz), an identifiable peak at around 6.8 kHz can be observed in the frequency spectra of both fuel mass fraction and heat release. This peak can also be found in the pressure spectra but it is weaker than the identifiable longitudinal acoustic modes. This response at high frequency corresponds to another hydrodynamic mode, the Precessing Vortex Core, the characteristics of which were introduced in Ref. 15. The representative responses of pressure, fuel and heat release fluctuations at PVC1 frequency are shown in Fig. 18. Evidence of a strong swirling flow can be seen in the cross-sectional view of each variable. The flow swirls at a high rate azimuthally while, in the axial direction, the top and bottom distributions are observed to be out-of-phase, which indicates a swirling core pattern in the diverging section. The influence of the PVC mode on the acoustic field is mainly concentrated in the diverging section and has a much weaker effect on the acoustic field in the combustor downstream of the dump plane. The swirling pattern present in the pressure mode shape indicates that the flow dynamics plays a more important role on the pressure than acoustics.

In the single LDI element configuration, the presence of hydrodynamic responses due to geometric effects and flow conditions can also potentially interact with the acoustic field in the combustor through nonlinear coupling. The evidence of that can be inferred from the peak standing at 4.5 kHz in the DMD frequency spectrum shown in Fig. 15. That frequency is close to the difference between PVC1 and 6L frequencies ($f_{\text{nonlinear}} = f_{\text{PVC1}} - f_{\text{6L}}$). The presence of nonlinear coupling in a premixed swirling flow combustor was discussed in Ref. 18. Representative responses at the nonlinear coupled frequency are shown in Fig. 19. Both the characteristics of longitudinal acoustic modes and PVC modes can be found in the plots. In the three cross-sectional views in Fig. 19, dominant swirling motions can be identified, which suggest the influence of flow field. In the sectional views, pressure shows a clear 13L mode shape in the combustor and, unlike the PVC modes, in Fig. 18, an equal weighting between the longitudinal acoustics and the PVC pressure mode can be observed her. For the fuel mass fraction and heat release, the influence of the acoustic modes is not easily identifiable and the spatial distributions of both still follow a swirling pattern with some compression in the axial direction, which might suggest potential acoustics coupling.

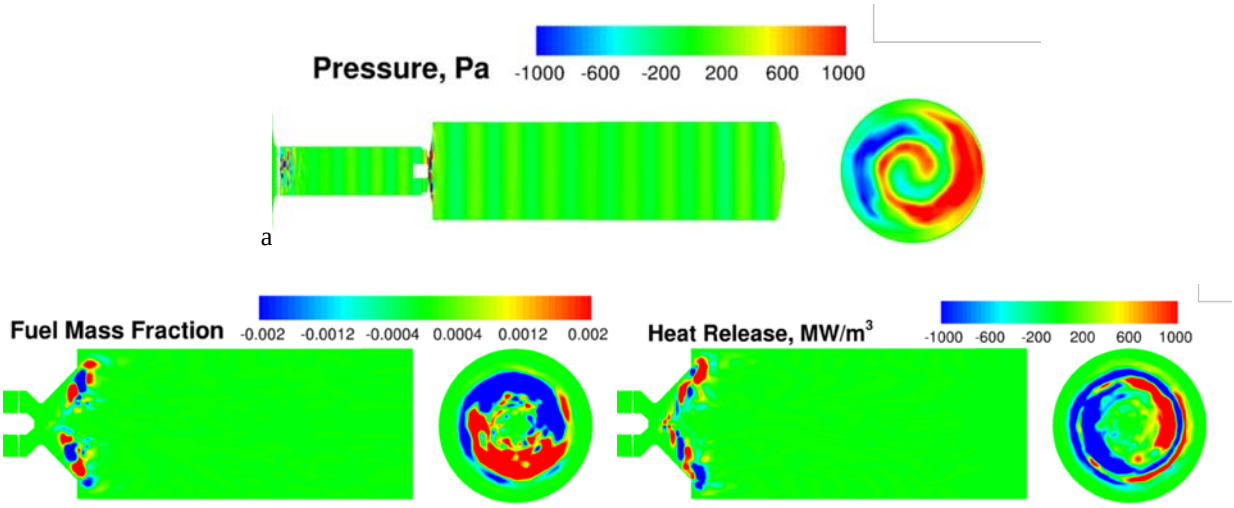

Figure 18. Representative reconstructed DMD responses at PVC1 frequency for closed geometry simulation for Φ = 0.36 T_{air} = 800K (fluctuations of top: pressure; bottom left: fuel mass fraction; bottom right: heat release).

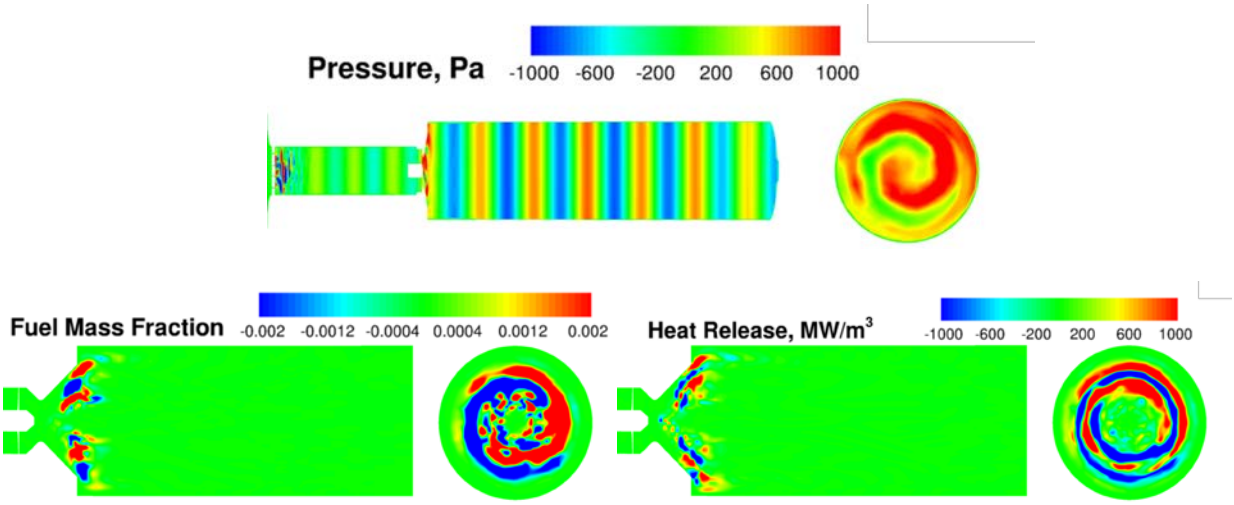

Figure 19. Representative reconstructed DMD responses at nonlinear coupled frequency for closed geometry simulation for Φ = 0.36 T_{air} = 800K (fluctuations of top: pressure; bottom left: fuel mass fraction; bottom right: heat release).

IV. Summary and Conclusions

Concurrent experimental and computational investigations have been performed on a laboratory single-element LDI gas turbine combustor to identify important mechanisms that sustain combustion instability. Both investigations are performed with the same geometry and operating conditions. Studies are done at both high and low equivalence ratios and reasonable agreement has been reached between experiment measurements and the computed results in terms of pressure peak-to-peak amplitudes and the dominant acoustic frequencies.

Simulations at the lower equivalence ratio show better agreement with the experiments and this case is selected for more detailed study to help elucidate the underlying physical interactions. Further, an acoustically-open geometry is also simulated to investigate important natural hydrodynamic modes present in the LDI configuration. A Vortex Breakdown Bubble (VBB) mode is clearly identified in the computed results. During the growth of VBB, fuel and combustion distributions are restricted in the diverging section due to the strong effects of the amplified reverse flow; while during the breakdown of the VBB, the distributions are more stretched and extended into the combustor with strong entrainment of fuel towards the centerline. VBB frequencies are quantified by DMD analysis and higher harmonics of VBB modes are found to interact with the higher harmonics of acoustic modes, which indicates the possibility of related coupling.

Studies of the acoustically-closed geometry simulation are performed using both cycle and DMD analysis. A single 6L cycle is selected to help identify the instability mechanisms. During the acoustic expansion process, the Weber number of the fuel spray decreases and larger-size drops are present in the diverging section due to reduced levels of secondary atomization. In turn, this leads to a slowdown of the fuel spray vaporization, and consequently to lower heat release. During the compression process, on the other hand, the gas phase axial velocity reaches its maximum. Weber number increases and the large-size drops break up more effectively into small ones. Fuel spray vaporization is enhanced as is the heat release. Moreover, the vortex breakdown bubble grows to its maximum and keeps pushing gaseous fuel to oxidizer side. The axial flow is amplified in the reverse direction, while the swirling flow is accelerated in the azimuthal direction. The accelerated flow enhances the mixing between fuel and oxidizer, which further increases the amount of heat release.

DMD analyses of the closed geometry simulations help establish a more quantitative understanding of the instability mechanisms. Azimuthally-uniform ring-like structures are identified at the dominant acoustic frequencies (5L and 6L), which indicate the strong driving force of the longitudinal acoustic field. Double peaks are found in low frequency region corresponding to the 1L (330Hz) and VBB1 (400Hz) frequencies. Mode shapes of 1L are similar to those of 5L and responses at the VBB1 frequency are similar to those found in the open geometry simulation. Comparing the results of the open and closed geometries, we observe that fundamental frequency of VBB is reduced due to the influence of the acoustic field. The updated VBB harmonics strongly suggest the direct coupling between 4^{th} and 5^{th} harmonics of the VBB mode with the 5^{th} and 6^{th} longitudinal acoustic modes respectively. This coupling between the 1L and VBB1 modes can help explain the pressure amplitude modulations observed in both the measured and computed pressure results. In high frequency region, an additional mode correspond to the Precessing Vortex Core (PVC) is identified as a fast and compact swirling motion in the diverging section of venture. The PVC frequency corresponds to the dominant peaks between 6,000 and 8,000Hz and is often observed in the parametric experiment studies. The influence of the PVC mode is restricted to the venturi section of LDI combustor. Finally, peaks observed between the dominant acoustic modes and the PVC mode indicate the presence of nonlinear coupling in the LDI combustor.

Acknowledgments

The authors acknowledge the support of the NASA Glenn Research Center under NASA Research Announcement (NRA) grant number NNX11AI62A, with Technical Monitor Mr. Kevin Breisacher and Program Manager Ms Julie Fowler. We would like to give special thanks to Dr. Charles Merkle who set the original direction of the study, Dr. Phil Lee of Woodward for providing the fuel nozzle used in the experiment, and Prof. Hukam Mongia of Purdue and Dr. Clarence Chang of NASA Glenn Research Center for technical advice.

References

1. Andrews, G.E., et al., *High-Intensity Burners with Low Nox Emissions.* Proceedings of the Institution of Mechanical Engineers, Part A: Journal of Power and Energy, 1992. **206**(1): p. 3-17.

2. Alkabie, H., Andrews, G. and Ahmad, N., *Lean Low NOx Primary Zones Using Radial Swirlers, paper ASME 88-GT-245*. in *ASME Gas Turbine and Aero Engine Congress and Exposition*. 1988.

3. Robert, T., *Low NO(x) potential of gas turbine engines,* in *28th Aerospace Sciences Meeting*. 1990, American Institute of Aeronautics and Astronautics.

4. Cooper, C.S. and Laurendeau, N.M., *Quantitative measurements of nitric oxide in high-pressure (2–5 atm), swirl-stabilized spray flames via laser-induced fluorescence.* Combustion and Flame, 2000. **123**(1–2): p. 175-188.

5. Cai, J., Jeng, S.M., and Tacina, R., *Multi-swirler aerodynamics - Experimental measurements,* in *37th Joint Propulsion Conference and Exhibit*. 2001, American Institute of Aeronautics and Astronautics.

6. Choi, K. and Tak, G., *Experimental studies of mixing effects on LDI combustion,* in *40th AIAA Aerospace Sciences Meeting & Exhibit*. 2002, American Institute of Aeronautics and Astronautics.

7. Robert, T., Chien-Pei, M., and Changlie, W., *Experimental Investigation of a Multiplex Fuel Injector Module for Low Emission Combustors,* in *41st Aerospace Sciences Meeting and Exhibit*. 2003, American Institute of Aeronautics and Astronautics.

8. Jun, C., San-Mou, J., and Robert, T., *The Structure of a Swirl-Stabilized Reacting Spray Issued from an Axial Swirler,* in *43rd AIAA Aerospace Sciences Meeting and Exhibit*. 2005, American Institute of Aeronautics and Astronautics.

9. Yongqiang, F., San-Mou, J., and Robert, T., *Confinement Effects on the Swirling Flow Generated by a Helical Axial Swirler,* in *44th AIAA Aerospace Sciences Meeting and Exhibit*. 2006, American Institute of Aeronautics and Astronautics.

10. Yi, T. and Santavicca, D.A., *Flame Spectra of a Turbulent Liquid-Fueled Swirl-Stabilized Lean-Direct Injection Combustor.* Journal of Propulsion and Power, 2012. **25**(5): p. 1058-1067.

11. Tongxun, Y. and Domenic, S., *Combustion Instability in a Turbulent Liquid-Fueled Swirl-Stabilized LDI Combustor,* in *45th AIAA/ASME/SAE/ASEE Joint Propulsion Conference & Exhibit*. 2009, American Institute of Aeronautics and Astronautics.

12. Tongxun, Y. and Domenic, S., *Flame Spectra of a Turbulent Liquid-Fueled Swirl-Stabilized LDI Combustor,* in *47th AIAA Aerospace Sciences Meeting including The New Horizons Forum and Aerospace Exposition*. 2009, American Institute of Aeronautics and Astronautics.

13. Bourgouin, J.-F., et al., *Sensitivity of swirling flows to small changes in the swirler geometry.* Comptes Rendus Mécanique, 2013. **341**(1–2): p. 211-219.

14. Moeck, J.P., et al., *Nonlinear interaction between a precessing vortex core and acoustic oscillations in a turbulent swirling flame.* Combustion and Flame, 2012. **159**(8): p. 2650-2668.

15. Syred, N., *A review of oscillation mechanisms and the role of the precessing vortex core (PVC) in swirl combustion systems.* Progress in Energy and Combustion Science, 2006. **32**(2): p. 93-161.

16. Candel, S., et al., *Dynamics of Swirling Flames.* Annual Review of Fluid Mechanics, 2014. **46**(1): p. 147-173.

17. Candel, S., et al., *Progress and challenges in swirling flame dynamics.* Comptes Rendus Mécanique, 2012. **340**(11–12): p. 758-768.

18. Palies, P., et al., *Nonlinear combustion instability analysis based on the flame describing function applied to turbulent premixed swirling flames.* Combustion and Flame, 2011. **158**(10): p. 1980-1991.

19. Palies, P., et al., *The combined dynamics of swirler and turbulent premixed swirling flames.* Combustion and Flame, 2010. **157**(9): p. 1698-1717.

20. Stöhr, M., Arndt, C.M., and Meier, W., *Effects of Damköhler number on vortex–flame interaction in a gas turbine model combustor.* Proceedings of the Combustion Institute, 2013. **34**(2): p. 3107-3115.

21. M, S., et al., *Experimental study of vortex-flame interaction in a gas turbine model combustor*. Combust. Flame, 2012. **159**: p. 2636.

22. Stöhr, M., Sadanandan, R., and Meier, W., *Phase-resolved characterization of vortex–flame interaction in a turbulent swirl flame.* Experiments in Fluids, 2011. **51**(4): p. 1153-1167.

23. Stöhr, M., et al., *Dynamics of lean blowout of a swirl-stabilized flame in a gas turbine model combustor*. Proceedings of the Combustion Institute, 2011. **33**(2): p. 2953-2960.

24. Steinberg, A.M., et al., *Flow–flame interactions causing acoustically coupled heat release fluctuations in a thermo-acoustically unstable gas turbine model combustor*. Combustion and Flame, 2010. **157**(12): p. 2250-2266.

25. Sweeney, M.S., et al., *Multiply conditioned analyses of stratification in highly swirling methane/air flames.* Combustion and Flame, 2013. **160**(2): p. 322-334.

26. Kim, K.T. and Santavicca, D.A., *Interference mechanisms of acoustic/convective disturbances in a swirl-stabilized lean-premixed combustor*. Combustion and Flame, 2013. **160**(8): p. 1441-1457.

27. de la Cruz García, Mastorakos, M., E., and Dowling, A.P., *Investigations on the self-excited oscillations in a kerosene spray flame.* Combustion and Flame, 2009. **156**(2): p. 374-384.

28. Providakis, T., et al., *Characterization of the coherent structures in swirling flames stabilized in a two-staged multi-injection burner: Influence of the staging factor*. Comptes Rendus Mécanique, 2013. **341**(1–2): p. 4-14.

29. Giuliani, F., et al., *Influence of pulsed entries on a spray generated by an air-blast injection device: An experimental analysis on combustion instability processes in aeroengines.* Proceedings of the Combustion Institute, 2002. **29**(1): p. 91-98.

30. Yu, Y.C., et al., *Effects of Mean Flow, Entropy Waves, and Boundary Conditions on Longitudinal Combustion Instability*. Combustion Science and Technology, 2010. **182**(7): p. 739-776.

31. Yen, Y., et al., *Examination of Spatial Mode Shapes and Resonant Frequencies Using Linearized Euler Solutions*, in *37th AIAA Fluid Dynamics Conference and Exhibit*. 2007, American Institute of Aeronautics and Astronautics.

32. Portillo, J., et al., *Application of a Generalized Instability Model to a Longitudinal Mode Combustion Instability*, in *43rd AIAA/ASME/SAE/ASEE Joint Propulsion Conference & Exhibit*. 2007, American Institute of Aeronautics and Astronautics.

33. Gejji, R., Huang, C., Yoon, C., and Anderson, W., "A Parametric Study of Combustion Dynamics in a Single-Element Lean Direct Injection (LDI) Gas Turbine Combustor", *52nd Aerospace Sciences Meeting*, 13-17 January 2014, National Harbor, Maryland.

34. Lian, C. , Xia, G. and Merkle, C., "Solution-Limited Time Stepping to Enhance Reliability in CFD Applications," *Journal of Computational Physics,* vol. 228, pp. 4836-4857, 2009.

35. Li, D., Xia, G. Sankaran, V. and Merkle, C., "Computational Framework for Complex Fluids Applications," in *3rd International Conference on Computational Fluid Dynamics*, Toronto, Canada, 2004.

36. Xia, G., Sankaran, V., Li, D. and Merkle, C., "Modeling of Turbulent Mixing Layer Dynamics in Ultra-High Pressure Flows," in *36th AIAA Fluid Dynamics Conference and Exhibit*, San Francisco, CA, 2006.

37. Lian, C., Xia, G. and Merkle, C., "Impact of Source Terms on Reliability of CFD Algorithms," *Computers and Fluids*, vol. 39, pp. 1909-1922, June 2010.

38. Li, D., Sankaran, V., Merkle, C. and Lindau, J., "A Unified Computational Formulation for Multi-Component and Multi-Phase Flows," in *43rd AIAA Aerospace Sciences Meeting and Exhibit*, 2005.

39. Spalart, P., Jou, W., Strelets, M. and Allmaras, S., "Comments on the feasibility of LES for wings on a hybrid RANS-LES approach," in *1st U.S. Air Force Office of Scientific Research Office Conference on DNS/LES*, Columbus, OH, 1997.

40. Travin, A., Shur, M. and Splart, P., "Physical and numerical upgrades in the detached-eddy simulation of complex turbulent flows," in *412 EUROMECH Colloquium on LES of Complex Transitional and Turbulence Flows*, Munich, 2000.

41. Wilcox, D., Turbulence Modeling for CFD, 2nd ed., La Cañada: DCW Industries, 1998.

42. Wilcox, D., "Formulation of the k-ω turbulence model revisited," in *45th AIAA Aerospace Sciences Meeting and Exhibit*, Reno, NV, 2007.

43. Westbrook, C., and Dryer, F., "Simplified Reaction Mechanisms for the Oxidation of Hydrocarbon Fuels in Flames," *Combustion Science and Technology*, vol. 27, pp. 31-43, 1981.

44. Yoon, C., Gejji, R., Anderson, W.E., and Sankaran, V., "Effects of Fuel Spray Modeling on the Combustion Dynamics of Lean Direct Injection Model Combustor", *ILASS-American 25th Annual Conference on Liquid Atomization and Spray Systems*, Pittsburgh, PA, May 2013.

45. Yoon, C., Huang, C., Gejji, R., Anderson, W.E., and Sankaran, V., "Computational Investigation of Combustion Instabilities in a Laboratory-Scale LDI Gas Turbine Engine", *49th AIAA/ASME/SAE/ASEE Joint Propulsion Conference*, July 14-17, 2013, San Jose, CA.

46. Huang, C., Yoon, C., Gejji, R. Anderson, W.E., and Sankaran, V., "Computational Study of Combustion Dynamics in a Single-Element Lean Direct Injection Gas Turbine Combustor", *52nd Aerospace Sciences Meeting*, 13-17 January 2014, National Harbor, Maryland.

47. Ashraf, I., and Jog, M. A., "Nonlinear breakup model for a liquid sheet emanating from a pressure-swirl atomizer," *Journal of Engineering for Gas Turbines and Power-Transactions of the Asme*, vol. 129, pp. 945-953, Oct 2007.

48. Senecal, P. K., Schmidt, D. P., Nouar, I., Rutland, C. J., Reitz, R. D., and Corradini, M. L., "Modeling high-speed viscous liquid sheet atomization," vol. 25, pp. 1073-1097, 1999/11// 1999.

49. O'Rourke, P. J., and Amsden, A. A., "The Tab Method for Numerical Calculation of Spray Droplet Breakup," 1987.

50. Beale, J. C., and Reitz, R. D., "Modeling spray atomization with the Kelvin-Helmholtz/Rayleigh-Taylor hybrid model," Atomization and Sprays, vol. 9, pp. 623-650, Nov-Dec 1999.

51. Han, Z. Y., Parrish, S., Farrell, P. V., and Reitz, R. D., "Modeling atomization processes of pressure-swirl hollow-cone fuel sprays," Atomization and Sprays, vol. 7, pp. 663-684, Nov-Dec 1997.

52. Patterson, M. A. and Reitz, R. D., "Modeling the effects of fuel spray characteristics on diesel engine combustion and emission," 1998.

53. Schmid, P., "Dynamic Mode Decomposition of Numerical and Experimental Data," *Journal of Fluid Mechanics*, vol. 656, pp. 5-28, August 2010.

54. Huang, C., Harvazinski, M., Anderson, W., and Sankaran, V., "Analysis of Self-excited Combustion Instability using Decomposition Techniques," in *51st AIAA ASM Including the New Horizons Forum and Aerospace Exposition*, Grapevine, TX, 2013.